Tectonics

RESEARCH ARTICLE
10.1029/2019TC005845

Key Points:
- Two main structural trends in the proximal domain of the northern SCS rifted margin
- The rift structure and evolution was significantly influenced by reactivation of two pre-existing basement fault systems
- Change of the regional extension direction from Syn-rift 1 to Syn-rift 2 indicated by reactivation pattern of pre-existing fault systems

Supporting Information:
- Supporting Information S1

Correspondence to:
L. Mei,
lfmei@cug.edu.cn

Citation:
Ye, Q., Mei, L., Shi, H., Du, J., Deng, P., Shu, Y., & Camanni, G. (2020). The influence of pre-existing basement faults on the Cenozoic structure and evolution of the proximal domain, northern South China Sea rifted margin. *Tectonics*, *39*, e2019TC005845. https://doi.org/10.1029/2019TC005845

Received 30 AUG 2019
Accepted 10 FEB 2020
Accepted article online 12 FEB 2020

The Influence of Pre-existing Basement Faults on the Cenozoic Structure and Evolution of the Proximal Domain, Northern South China Sea Rifted Margin

Qing Ye[1], Lianfu Mei[1], Hesheng Shi[2], Jiayuan Du[2], Peng Deng[1], Yu Shu[2], and Giovanni Camanni[3]

[1]Key Laboratory of Tectonics and Petroleum Resources, Ministry of Education, China University of Geosciences, Wuhan, China, [2]Shenzhen Branch of the China National Offshore Oil Corporation, Shenzhen, China, [3]DiSTAR, Università degli Studi di Napoli "Federico II", Naples, Italy

Abstract In this paper, we investigate the structure of the Cenozoic rift basin in the proximal domain of the northern South China Sea (SCS) margin, with an emphasis on the influence exerted by pre-existing basement faults on rift development. Results of our work indicate that the overall rift architecture of the proximal domain of the northern SCS margin is associated with extensional faults arranged in two main structural trends, WNW- to EW-trending and ENE-trending. Structural evidence presented in this paper suggests that extensional faults of the two main structural trends mainly reactivated two pre-existing basement fault systems mapped in previous works, a WNW- to EW-striking thrust fault system (PFS1) and an ENE-striking thrust fault system (PFS2). During the first rifting phase, both pre-existing fault systems were reactivated; however, strains and depocenters were mainly localized on the ENE-striking normal fault system that reactivated the PFS2. On the contrary, in the second rifting phase, extension was mainly accommodated by WNW- to EW-striking normal faults that reactivated the PFS1, while most of the earlier ENE-striking normal faults became inactive or less active. These different degrees of reactivation of the two pre-existing fault systems during the two rifting phases suggest a clockwise rotation of the regional extension direction from NNW-SSE in the Syn-rift stage 1 to N-S in the Syn-rift stage 2. This study implies that apart from Cenozoic tectonic processes, pre-existing structures have also played a key role during rifting evolution across the SCS margin.

1. Introduction

The South China Sea (SCS), the largest marginal sea in the western Pacific region, developed as the result of Cenozoic rifting and seafloor spreading on the South China margin (Figure 1). During the past 5 years, the SCS area has been one of the most studied rift systems worldwide not only for its rich hydrocarbon resources but also for its unique tectonic location that makes it an ideal laboratory for studying and testing modes of lithospheric extension and breakup. For these reasons, the SCS area has been the object of investigation of the International Ocean Discovery Program (IODP) expeditions 349 in 2014, and 368 and 369 in 2017 (Figure 1a). These latest studies, focusing on either the distal or oceanic domains, have made significant progresses in understanding the mechanisms of lithosphere thinning during continental breakup, and the ages and pattern of the subsequent sea-floor spreading process of the SCS (e.g., Expedition 349 Scientists, 2014; Li et al., 2014; Jian, et al., 2018; Sun et al., 2018; Larsen et al., 2018). However, mainly due to the confidentiality and/or nonavailability of inner-basin high-resolution seismic reflection data, a comprehensive basin-scale model of the rift structure and evolution of the SCS margin that includes its proximal domain has not been proposed yet. The structure of this proximal part of the rifted margin is only described in old studies based on regional gravity and magnetic data, or on sparse 2D seismic data with limited resolution (e.g., Pigott & Ru, 1994; Ru & Pigott, 1986; Zhou et al., 1995).

Nevertheless, over the past few years, extensive exploration for hydrocarbons in the Cenozoic Pearl River Mouth Basin (PRMB) had led to the acquisition of a considerable number of boreholes and high-resolution 3D seismic reflection data, especially in the proximal domain of the northern SCS margin. These data make feasible a more precise interpretation and mapping of major stratigraphic interfaces and rifting faults and therefore a thorough investigation of the rift structure. Important for this paper, a recent study based on

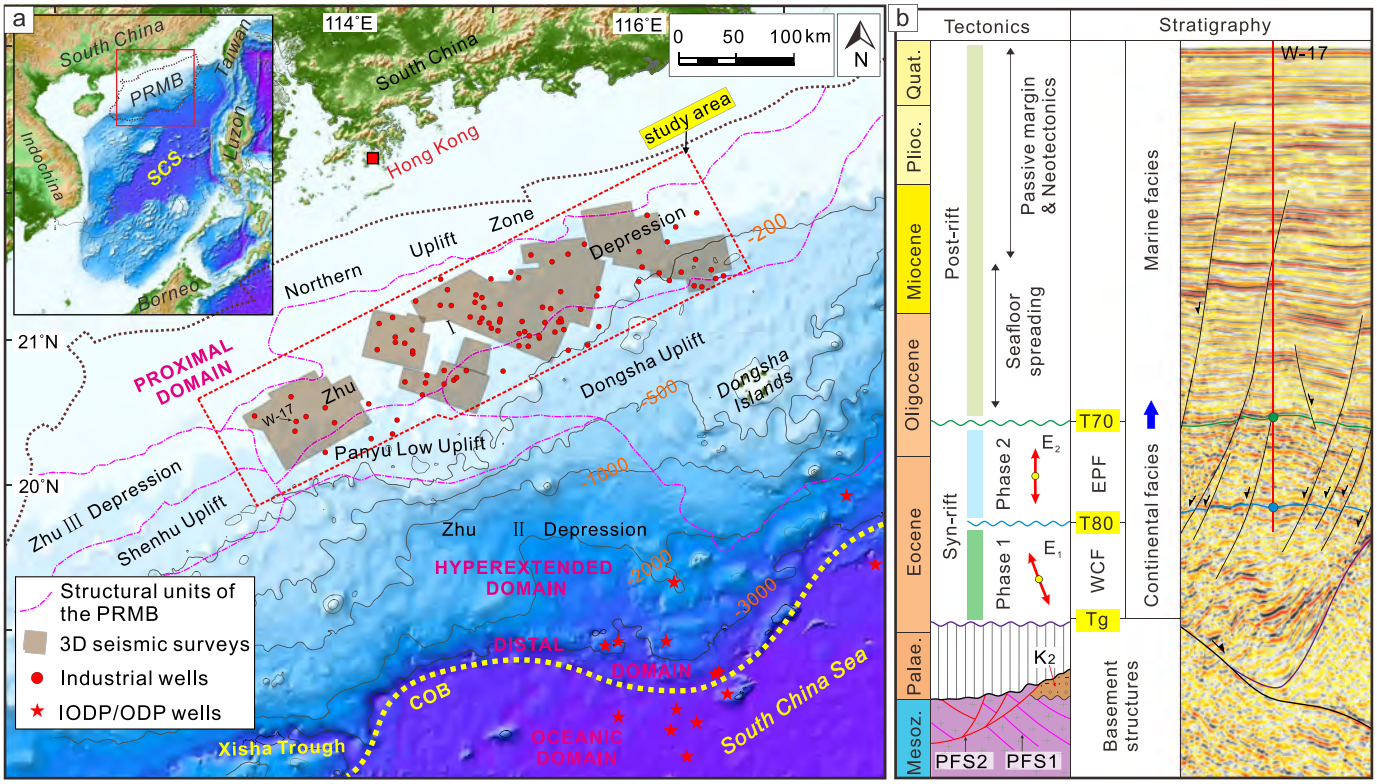

Figure 1. (a) Bathymetric map of the northern South China Sea margin showing structural location of the study area and the main datasets used in this study (2D seismic surveys are not shown). SCS—South China Sea; PRMB—Pearl River Mouth Basin; COB—continent-ocean boundary. (b) Summary of tectono-sedimentary evolution of the study area. PFS1 and PFS2 are two major pre-existing fault systems within basement. WCF—Wenchang Formation; EPF—Enping Formation. Tg, T80, and T70 are the names of key seismic horizons that bound the syn-rift units. E1 and E2 are the extensional directions during the two rifting phases.

these high-resolution 3D seismic data revealed a complex network of pre-existing faults within the basement of the Cenozoic rift basin in the northern SCS margin (Ye, Mei, Shi, Camanni, et al., 2018). Therefore, how this region of the Cenozoic rift basin evolved to its current architecture needs to be reconsidered from the perspective of basement control since it is well known in rift basins worldwide that pre-existing basement structure is a key factor in shaping the rift architecture and influencing the kinematic evolution of rifting (e.g., Autin et al., 2013; Bird et al., 2015; Bladon et al., 2015; Bonini et al., 2015, 2016; Corti et al., 2007; Fazlikhani et al., 2017; Gibson et al., 2013; Katumwehe et al., 2015; Kharazizadeh et al., 2017; Manatschal et al., 2015; Phillips et al., 2016; Rotevatn et al., 2018).

Building on previous results (i.e., Ye, Mei, Shi, Camanni, et al., 2018), in this paper, we carry out a study of the Cenozoic rift structure in the proximal domain of the northern South China Sea margin based on an analysis of high-resolution industrial 3D seismic reflection data and wells. An emphasis is placed on how and to what degree pre-existing basement faults have influenced the rift development. Results of this study may help to gain some new insights into the development mechanisms of the Cenozoic rift architecture in the proximal domain of northern SCS margin and may also have significant implications for a better understanding of rifting evolution in adjacent regions across the SCS margin. Importantly, results of this study allow to make some consideration on the changes of the extension directions at different rifting phases, a still controversial issue in the SCS area, whose analysis may have regional implications for deciphering the dynamic origin and kinematic development of the SCS opening.

2. Geological Setting

2.1. Location of the Study Area

The NE-oriented Pearl River Mouth Basin (PRMB) is the largest Cenozoic rift basin on the northern margin of the SCS (Figure 1a). The study area of this paper is an approximately 400-km-long and 100-km-wide

elongated rifted zone (named the Zhu I Depression), which is a part of the PRMB and confined to the north with the Northern Uplift Zone and to the south with the Panyu lower uplift and Dongsha uplift (Figure 1a). The study area comprises a significant portion of the proximal domain, that is, the landward, outboard area, of the northern SCS rifted margin (e.g., Yang et al., 2018; Zhou et al., 2018). The continental crust of this domain was stretched at low values of extension and characterized by classical graben and half-graben basins filled with wedge-shaped syn-tectonic stratigraphic units (Peron-Pinvidic et al., 2013). The average crustal thickness of the study is around 25 km (e.g., Yan et al., 2001; Tsai et al., 2004; Hayes & Nissen, 2005; Zhang et al., 2008). The water depth of this domain is less than 500 m (Figure 1a).

2.2. Cenozoic Tectono-Sedimentary Evolution

The SCS oceanic basin developed in response to diachronous continental break-up processes from the Late Oligocene to Middle Miocene (~32–15.5 Ma) (e.g., Briais et al., 1993; Li et al., 2014). The continental rifting prior to continental breakup was also diachronous along the margin and started earlier in the eastern basins and then propagated westwards (e.g., Franke et al., 2014; Savva et al., 2014; Morley, 2016a). In a similar fashion to other rift basins, the PRMB has experienced multiphase extension during the continental rifting stage (e.g., Deng, 2018; Li, 1993; Li et al., 1999; Pigott & Ru, 1994; Ru & Pigott, 1986; Wu et al., 2016). Two main rifting phases, an early rifting phase in the early to middle Eocene and a late rifting phase from the Late Eocene to the early Oligocene, were reported by previous studies on the proximal domain (e.g., Wang et al., 2015; Zhu et al., 2016; Liu et al., 2016a, 2016b; Ge et al., 2017, 2018; Ye, Mei, Shi, Shu, et al., 2018). The syn-rift stratigraphic units in the study area are separated by three major horizons, that is, the Tg, the T80, and the T70 (Figure 1b). The Tg is the rift onset unconformity and also corresponds a regional unconformity between Mesozoic and Cenozoic throughout the whole SCS area. The T80 is a basin-wide unconformity and represents the boundary surface between the Syn-rift 1 and the Syn-rift 2 units. Finally, the T70 corresponds to the breakup time of the SCS and is also a basin-wide unconformity, which marks the end of the syn-rift stage in this region. The first phase of the rifting leads to the deposition of the Wenchang Formation, which mainly consists of grey to black organic-rich middle to deep lacustrine shale interbedded with sandstone; the second phase of the rifting is associated with the deposition of the Enping Formation, dominated by fluvial and shallow to middle lacustrine-paludal shale, sandstone, and thin coal beds (Liu et al., 2016a). These two syn-rift sequences are the major source rocks for hydrocarbon in the PRMB (e.g., Hesheng et al., 2015; Bao et al., 2017). Rifting ceased in this domain when continental breakup occurred and seafloor spreading started in the SCS at ca. 32 Ma, and the basin entered into the post-rift stage. During this latter stage, the sedimentary deposition switched from continental facies to marine facies. The post-rift stage was influenced by neotectonics, associated with faulting, magmatism, and uplifting (e.g., Deng et al., 2018; Lüdmann et al., 2001; Sun et al., 2014; Wu et al., 2014; Ye et al., 2017).

2.3. Pre-existing Basement Fault Systems

The proximal domain of the SCS rifted margin was mainly established on a basement comprising the Late Mesozoic arc-related granitoids, and few sedimentary and volcanic rocks (Figure 2a; e.g., Yi et al., 2012; Li et al., 2018; Ye, Mei, Shi, Shu, et al., 2018; Ye, Mei, Shi, Camanni, et al., 2018). A recent study from our research group recognized a complex network of pre-existing faults within the upper-crust basement in this region of the Cenozoic rift basin and related them to a multiphase Late Cretaceous tectonic evolution in the SCS area (Ye, Mei, Shi, Camanni, et al., 2018). In particular, two superimposed thrust fault systems, a WNW- to EW-striking one and an ENE-striking one, and fewer extensional faults were interpreted using large amounts of high-resolution 3D seismic reflection data (Figure 2a). The two pre-existing thrust fault systems strongly deformed the granitoid-dominated basement and constituted the main pre-existing structures within the basement. These two pre-existing fault and fracture systems are named PFS1 (WNW- to EW-striking) and PFS2 (ENE-striking) in this paper and are widely distributed within the basement of the study area and illuminated by prominent high-amplitude reflectors within seismic reflection data. The PFS1 was considered to have developed in a transpressional tectonic event at the Early-Late Cretaceous boundary; faults belonging to this fault system are mainly characterized by small spacing, and high dip angle, illuminated by dense continuous strong reflections on seismic sections (Ye, Mei, Shi, Camanni, et al., 2018). They dip both towards the SSW and the NNE, defining a doubly verging structure, and show a positive flower structure in section. The dashed black line in Figure 2a highlights the axis of such a regional doubly verging structure and separates a northern portion of N-verging thrusts from a southern portion of S-verging

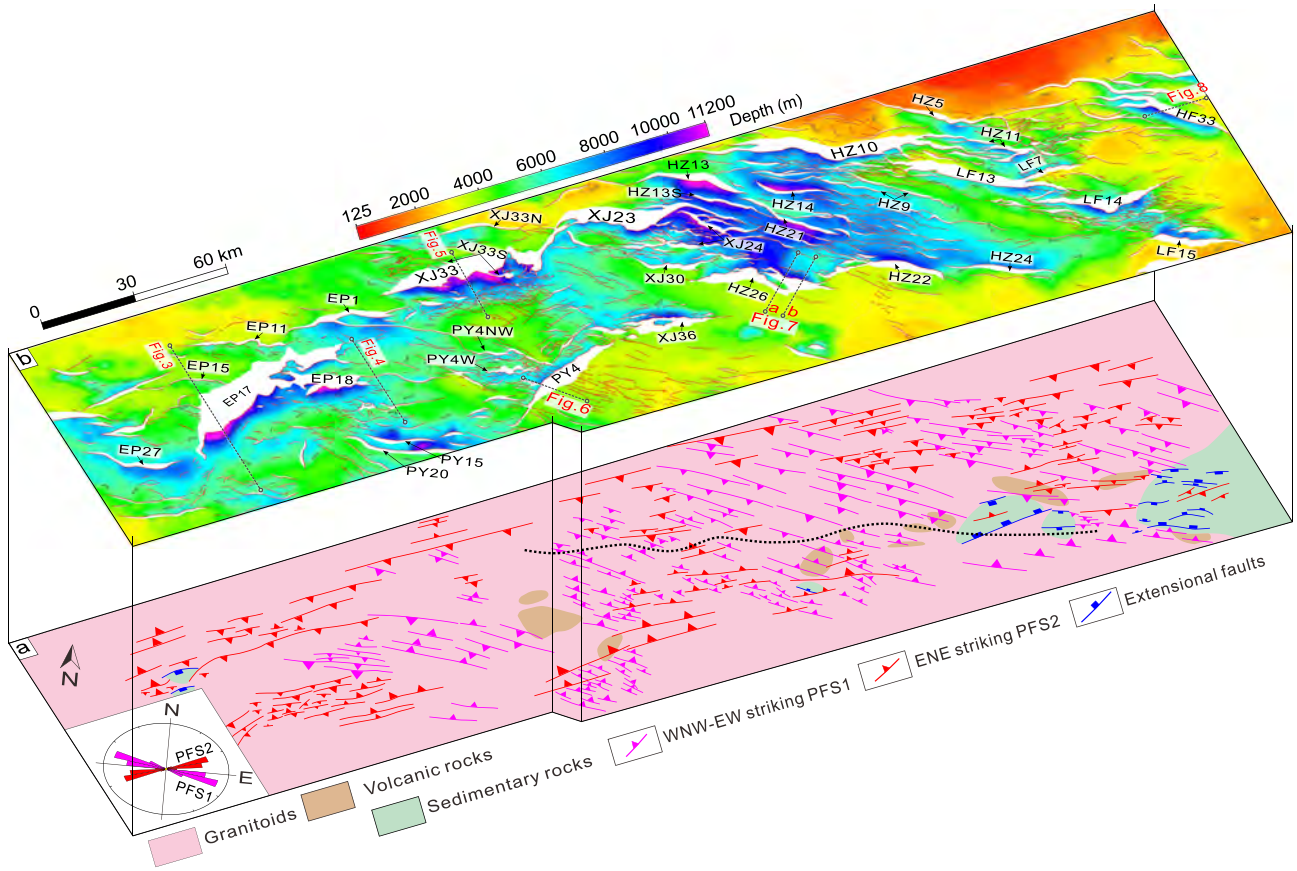

Figure 2. (a) Map of basement lithology and pre-existing basement faults of the study area (Ye, Mei, Shi, Camanni, et al., 2018). Two-phase thrust fault systems and one extensional fault system developed on the granitoids-dominated basement. The WNW- to EW-striking thrust fault system (PFS1) has an a regional doubly verging structure, and the dashed black line highlights the axis and separate a northern portion of N-verging thrusts form a southern portion of S-verging thrusts. The ENE-striking thrust fault system (PFS2) mainly dips SSE with few back-thrust faults developed. Fault strike azimuth frequency distribution of the two thrust fault system are illustrated as plot, which constitute the main pre-existing basement structures of the study area. (b) Depth-structure map of the base rift surface (i.e., the Tg Horizon) of the study area illustrating the general rift configuration. This map was mainly based on interpretation of 3D seismic data and supplemented by 2D seismic lines. The length and width of the fault polygons are generated using hanging wall and footwall cutoff points and identifying realistic along-strike fault heave patterns. Names of major bounding faults or fault groups are tagged. An additional plan view of the Figure 2b can be found in the supporting information.

thrusts. The PFS2 formed in the late stage of the Late Cretaceous, and its development has been related to ridge-push compression during the Proto-SCS opening (Ye, Mei, Shi, Camanni, et al., 2018). It was superimposed on the earlier PFS1 and largely crosscut and dissected the early ENE-striking thrust faults system both along strike and dip direction. Faults belonging to this thrust system are widely spaced, and have an overall low dip angle, and mainly dip towards the SSE though few back thrusts developed in some locations.

3. Data and Methods

The study area is entirely covered by 3D and 2D seismic reflection and well data (Figure 1a). All these 3D/2D seismic and well data were collected by the China National Offshore Oil Corporation (CNOOC) Shenzhen Branch and associated cooperative service companies over the past decade. The 3D seismic reflection data consist of 8 separate seismic volumes and cover a total area of over 2.4×10^4 km^2. These seismic volumes have a bin size of 12.5 × 12.5 m or 12.5 × 25 m, sample rates of 2 ms, and a dominant frequency of 30 Hz in average, which gives a vertical resolution of approximately 20 m. Most of these 3D seismic data provide exceptional images of not only the Cenozoic sedimentary cover but also the underlying structures within basement. More than 90 industrial wells have been collected, which were tied to the seismic data to help

the seismic interpretation. Time-depth conversion of the data was performed by using best-fit second-order polynomials derived from boreholes. For seismic sections presented in this paper, faults confined to the post-rift units are not extensively interpreted since the focus of this work is the syn-rift stage, and we also do not concentrate on the above-mentioned basement structures that have been done in a previous paper (Ye, Mei, Shi, Camanni, et al., 2018). A set of key structural maps, fault polygon maps, and isopach maps were produced to assess the rift architecture, depocenter development, and fault geometry and activity in different rifting phases.

4. Results

4.1. Overall Cenozoic Rift Architecture

The structural map of the base rift surface (i.e., the Tg Horizon) shows the overall Cenozoic rift architecture of the study area (Figure 2b). The complex fault network at this surface is mainly the result of the superposition of faults of the two rifting phases, and few post-rift faults in some structural highs with no syn-rift deposition, such as on southern margins of the rifted zone (the Dongsha Uplift Zone). The maximum depth of the top basement in the study area is approximately 8 km in its western part. The structure of the study area is defined by a complex arrangement of a number of half-grabens, grabens, and interposed structural highs. The whole NE-trending rifted zone is generally bounded by left-stepping en-echelon arranged sets of south- and north-dipping normal faults. Some large faults also developed in the interior of the rifted zone. Importantly for this paper, rift-related faults clearly exhibit two noncollinear structural trends, ENE-striking and WNW- to EW-striking. Furthermore, some of the major faults have complex geometries, displaying a "Z" shape (e.g., HZ26, XJ23, and HZ10) or "V" shape (e.g., LF14 and HF33) on the map.

4.2. Reactivation of Two Pre-existing Basement Fault Systems

The two noncollinear normal fault systems that can be identified on the structural map of the base rift surface resemble the structural orientation of the two pre-existing fault systems within the basement, suggesting a high degree of structural linkage between the underlying pre-existing basement structures and the Cenozoic rift fault system (Figure 2). Such structural linkage is manifested in widespread fault reactivation of both the PFS1 and PFS2 in seismic reflection data. Fault reactivation, besides being suggested by the similar orientation of rift-related and basement faults as mentioned above, is also demonstrated by rifted-related faults hard-linking downward to basement faults that along strike may become buried below the Tg unconformity strongly supporting the pre-existing nature of the faults. Furthermore, the en-echelon nature of a number of rift-related faults is also strongly suggestive of a model in which they arise from the reactivation of pre-existing faults (e.g., Morley et al., 2004). Fault reactivation, as has been well studied worldwide, is considered to be selective and usually influenced by a range of factors, such as, among others, the orientation of pre-existing faults in relation to regional extension direction, and the size and dip angle of the pre-existing faults (e.g., Daly et al., 1989; Williams et al., 1989; Sibson, 1985; Faccenna et al., 1995; Corti et al., 2006; Bonini et al., 2015, Reilly et al., 2016, Morley et al., 2016b). For these reasons, generally, only some of the pre-existing faults undergo reactivation, and for one single fault, the reactivation can even just take place in some portions of it. In our study area, two evidences are suggesting that the Cenozoic rifting faults have only partially reactivated the pre-existing faults: (i) partial portions of the Cenozoic rifting faults were not reactivated and buried below the Tg unconformity along strike; (ii) numerous nonreactivated fault planes are preserved within the foot-wall and hanging-wall basement blocks. Specific examples of fault reactivation in our study area are described in the next paragraph using some explanatory seismic sections.

The ENE-striking rifting faults, such as the major bounding faults EP17, XJ33, and PY4, mainly reactivated the ENE-striking thrust faults of the PFS2. For example, the EP17 fault comprises an approximately 53-km-long low angle normal fault segment (fault dip <30°) that partly reactivated a pre-existing thrust fault (Figure 3; Ye, Mei, Shi, Shu, et al., 2018). The fault plane of this fault remains nonreactivated and truncated by the Tg unconformity to the east (Figure 4), suggesting its pre-existing nature. The XJ33 fault also reactivated a preexisting thrust fault of the PFS2 though it was later crosscut by the E-W striking XJ33S fault (Figure 5). The NW-dipping PY4 fault reactivated one of the few back-thrust faults (NW-dipping) of the PFS2, and it merges downwards to an unreactivated thrust fault plane (Figure 6). Most of the WNW- to EW-striking normal faults reused pre-existing faults of the PFS1. For example, the eastern

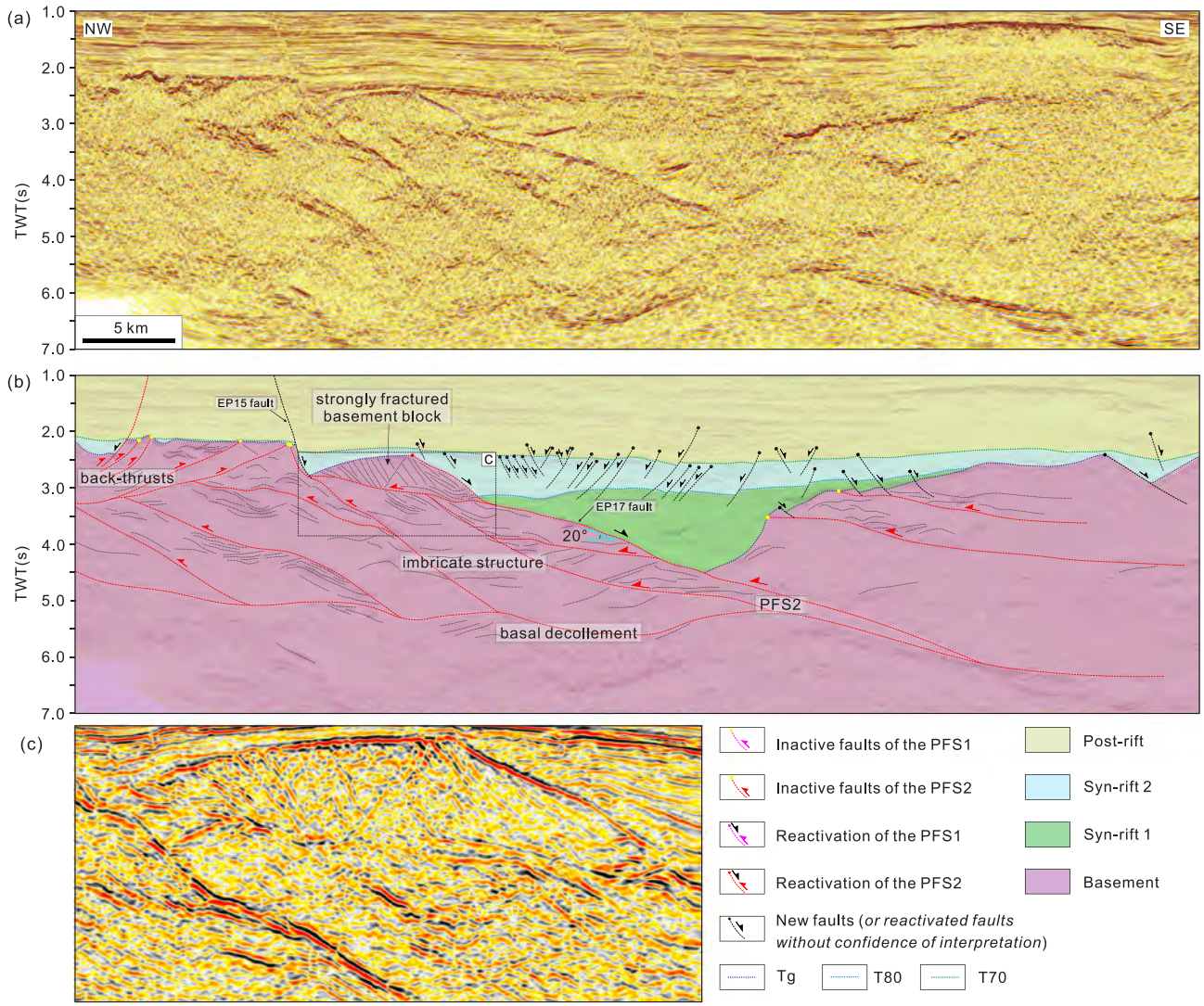

Figure 3. (a-b) Uninterpreted and interpreted seismic sections (see Figure 2b for location) mainly showing the typical feature of the PFS2 and Cenozoic reactivation in the west part of the study area. Faults confined within the basement and do not offset the Tg surface suggested their pre-rift nature. Imbricate structure and back-thrusts above the basal decollement are imaged. The EP17 fault is a low angle normal fault that partly reactivated a pre-existing thrust fault of the PFS2 as shown in Figure 4. Faults confined to the post-rift units are not extensively interpreted. (c) The basement block was strongly deformed with large number of pre-existing faults and fractures preserved within it.

portion of the HZ26 fault reactivated a set of pre-existing fault planes of the PFS1 (Figure 7), which is demonstrated by large numbers of nonreactivated fault planes within the hanging-wall basement with similar seismic reflection characteristics. The WNW-striking segment of the V-shape HF33 fault reactivated a pre-existing fault of the PFS1(Figure 8). Since the PFS1 was crosscut by faults of the PFS2, it is widespread in the study area that numerous fault planes of the PFS1 are preserved within the basement zones above or below fault planes of the PFS2 (Figures 4 and 5). For these cases, fault reactivation of the PFS1 could either crosscut or branched out of faults of the PFS2 with relatively low dip angle. For example, the EW-striking EP18 (Figures 2b and 4) branched out of the EWN-striking EP17 low-angle normal fault, while the WNW-striking XJ33S fault, which reactivated a pre-existing basement fault of the PFS1 below the XJ33 fault plane, crosscut the XJ33 fault (Figures 2b and 5). The map pattern of the two pre-existing fault systems has also significantly influenced basin-scale structure of the rifted zone. For example, the reactivation of the WNW-trending doubly verging structure of the PFS1 led to the development of a large graben system defined by symmetric NNE-dipping and SSW-dipping normal fault populations (Figure 2).

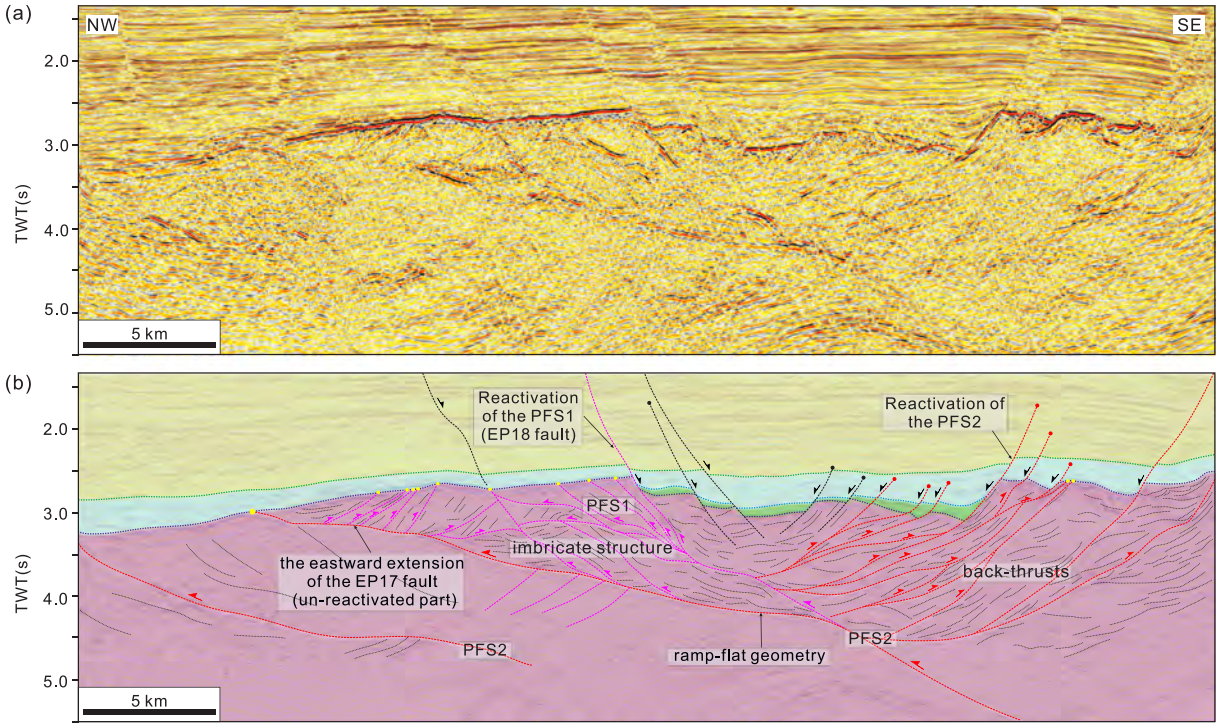

Figure 4. (a-b) Uninterpreted and interpreted seismic sections (see Figure 2b for location) showing the two pre-existing fault systems. The PFS1 was crosscut by faults of the PFS2. Faults of the two systems are difficult to be distinguished solely from the section, and they distinguish from each other mainly in fault strike on the map. Only some of the pre-existing faults was reactivated in the Cenozoic. The unreactivated fault with a ramp-flat geometry in this section is the eastward extension of a major thrust fault, which was reactivated by the EP17 fault in its western part as show in Figure 3b. The EP 18 fault, which reactivated the PFS1, branches out of the major thrust fault of the PFS2 at depth.

4.3. Cenozoic Rifting Evolution of the Proximal Domain of the Northern SCS Rifted Margin

The fault network at the base rift horizon arises from the superposition of faults that developed during different extensional phases, hence not reflecting their spatial-temporal evolution (Figure 2b). The isopach maps of Syn-rift 1 Wenchang Formation and the Syn-rift 2 Enping Formation allow us to investigate the distribution of depocenters through time and space (Figures 9 and 10) and provide detailed insights into the spatiotemporal change and migration of fault activity and strain localization.

4.3.1. First Rifting Phase

The first rifting phase took place during the early to middle Eocene and is characterized by numerous isolated depocenters within half-graben or graben systems located where subsidence rates were greater (Figure 9), in a similar fashion to the early development of many rift systems worldwide (e.g., Gawthorpe & Leeder, 2000). Extensional faults during this stage reactivated both the PFS1 and PFS2, which was suggested by the contemporaneous development of both the ENE-striking and WNW- to EW-striking normal fault systems, and some complex "Z" shape (e.g., HZ26, XJ23, and HZ10) and "V" shape (e.g., LF14 and HF33) fault geometries, along with their associated depocenters. It is clearly from seismic sections that during the Syn-rift stage 1, the EP17, XJ33, and PY4 faults reactivated the PFS2 (Figures 3, 5, and 6), while the EP18, the eastern portion of the HZ26 faults and the eastern portion of the HF33 faults reactivated the PFS1 (Figures 4, 7, and 8).

However, these two rifting fault systems with different strike show different degrees of fault activity at this first rifting stage, and the size and thickness of depocenters they controlled vary considerably (Figure 9). Most of the large and thick depocenters are associated with the ENE-striking normal faults (e.g., EP17, XJ33, PY4, LF15, eastern fault segment of HZ26, and eastern fault segment of HZ10), among which the thickest one is controlled by the EP17 fault. On the contrary, most of the depocenters associated with the WNW- to EW-striking normal faults are relatively smaller and thinner. More than 70% area with more than 2,000 m thickness deposition are controlled by the ENE-striking normal faults, while only 28% by the WNW-

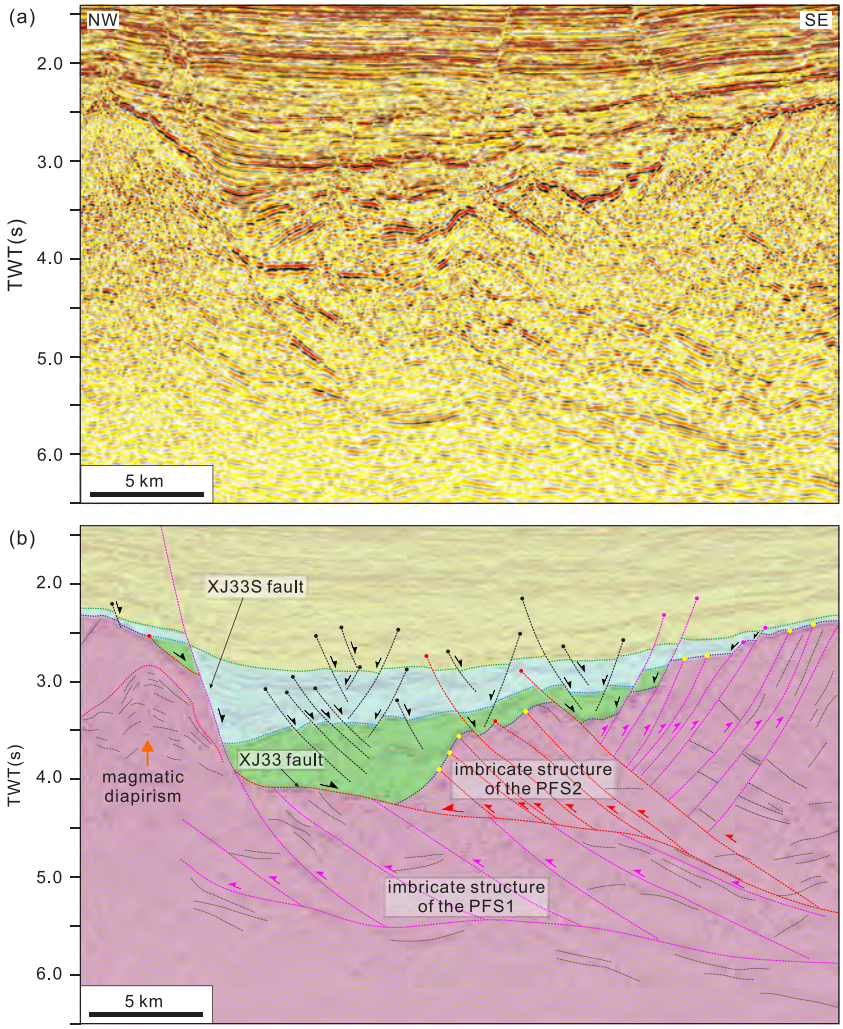

Figure 5. (a-b) Uninterpreted and interpreted seismic sections (see Figure 2b for location) across the XJ33 fault showing reactivation of the two pre-existing fault systems. Two superimposed imbricate structures of the two pre-existing thrust fault systems are imaged, and they were both partly reactivated during the Cenozoic rifting stage. The XJ33 fault reactivated a sole thrust fault of the ENE-trending PFS2 in the first rifting phase, while during the second rifting phase it became inactive and was crosscut by the XJ33S fault, which reactivated a pre-existing fault of the PFS1 within the basement below the XJ33 fault plane.

to EW-striking normal faults. Significant thickness difference even exists between adjacent depocenters respectively controlled by WNW-striking and ENE-striking portions of one single fault, such as the HZ10 and the XJ23 faults (Figures 9 and 11). The dominant activity of the ENE-striking rifting faults reflected the preferential reactivation of the PFS2 during the first rifting phase.

4.3.2. Second Rifting Phase

The second rifting phase, developed during the late Eocene to the early Oligocene, is associated with a rapid expansion of the rifted zone (Figure 10). For example, the northern margin of the rifted zone in the western part of the study area stepped northward to a set of new EW-striking faults (EP11, eastern segment of EP1, and XJ33N). The number of depocenters largely decreased, and many of the small depocenters in the early Syn-rift stage 1 grew in size and became more linked. In addition to these general changes, a major change from the first rifting phase to the second rifting phase is the different degrees of fault activity of the ENE-striking and the WNW- to EW-striking fault systems, and the migration of depocenters (Figure 10). The main depocenters migrated from mainly being controlled by ENE-striking normal faults in the Syn-rift stage 1 to being controlled by the WNW- to EW-striking normal faults in the Syn-rift stage 2. In detail, more than 90% area with more than 2,000 m thickness deposition were controlled by the WNW- to EW-striking

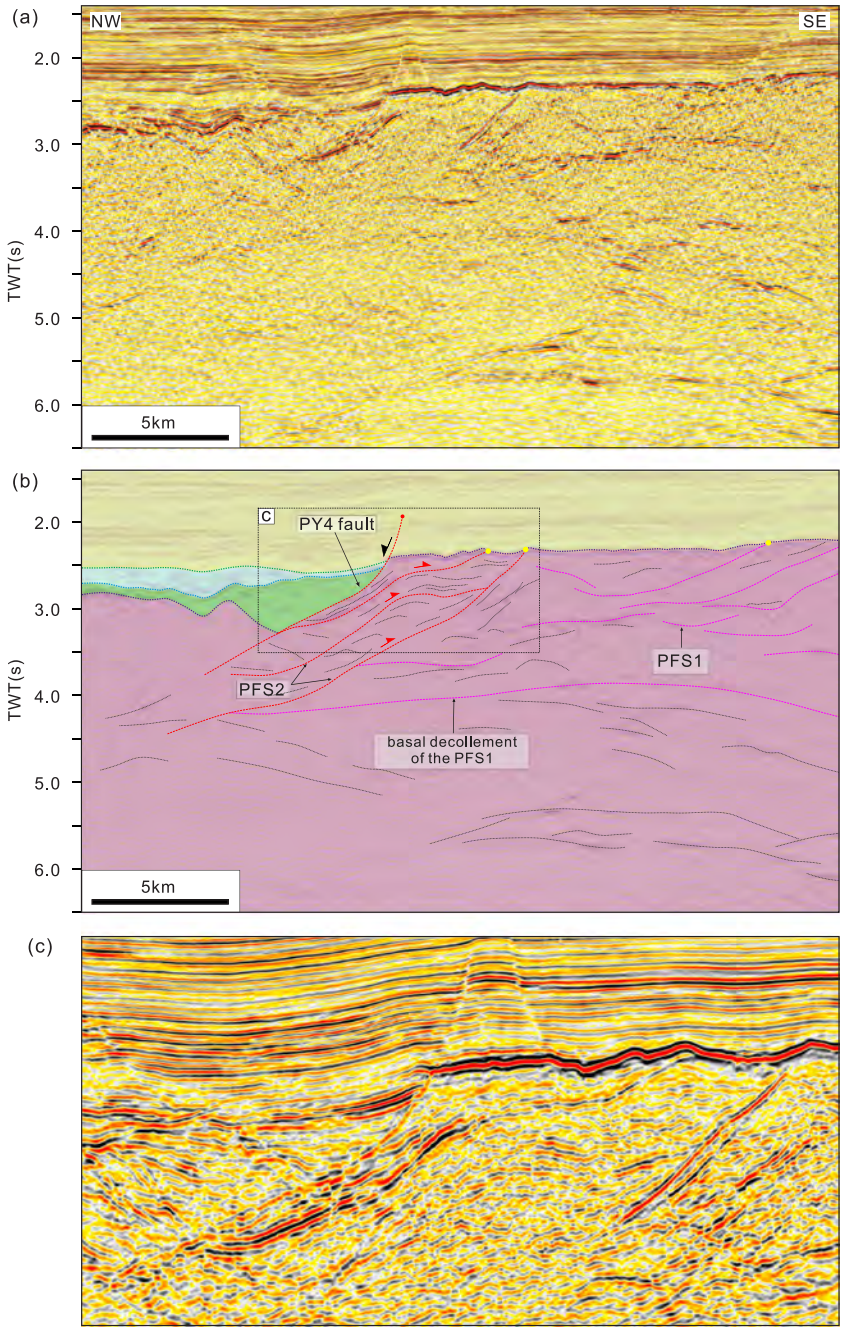

Figure 6. (a-b) Uninterpreted and interpreted seismic sections (see Figure 2b for location) across the PY4 fault. This section is NW-SE orientated, almost parallel to the trend of the PFS1. Faults of the PFS2 crosscut faults of the PFS1 including its basal decollement. The PY4 fault reactivated a pre-existing fault of the PFS2, and it merges downwards to an unreactivated thrust fault. (c) Detail with enlarged scale showing pre-existing faults of the PFS2 below the Tg unconformity.

bounding faults, which either reactivated the PFS1 in the Syn-rift stage 1 and largely increase their activity during the Syn-rift stage 2 (e.g., HZ13, XJ24, western segment of HZ10, HZ5, and HZ11), or directly reactivated the PFS1 in the Syn-rift stage 2 (e.g., EP20, EP27, PY20, XJ33N, and XJ33S). Particularly, the western WNW-striking portion of the HZ10 fault became more active than the eastern ENE fault portion of it, as shown by the relative thickness they controlled (Figures 10 and 11). The HZ13 fault, which was only a small fault during the Syn-rift stage 1, is associated with the thickest and largest depocenter

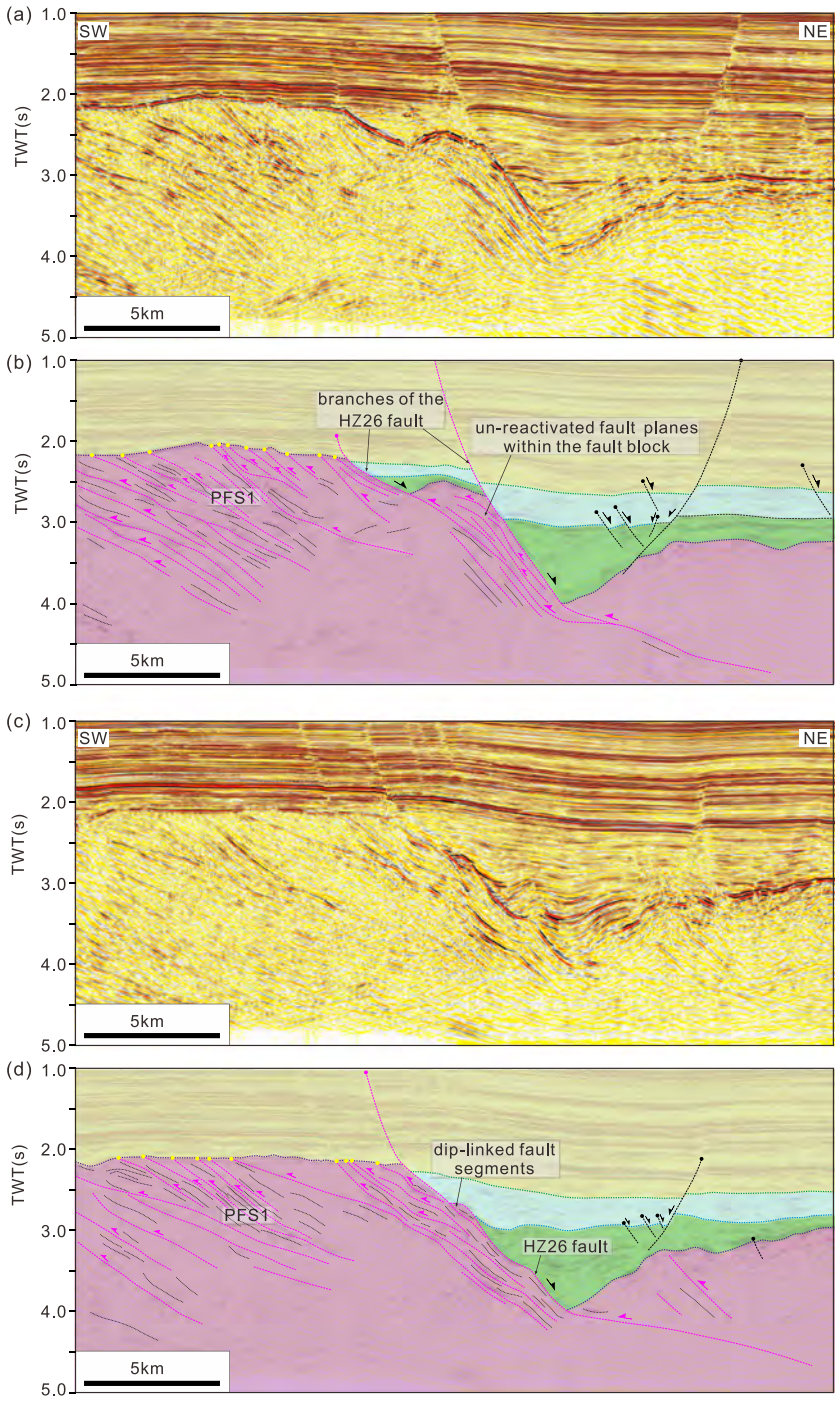

Figure 7. Two adjacent seismic sections (see Figure 2b for locations) across the eastern WNW-striking portion of the HZ26 fault showing typical features and partly reactivation of the PFS1. Large numbers of unreactivated pre-existing faults are well preserved within the hanging-wall basement zone. This portion of the HZ26 fault is consisted of a group of fault branches or segments, which reactivated a set of pre-existing faults of the PFS1.

(~3,500 m) during the Syn-rift stage 2. In contrast, many of the major Syn-rift 1 ENE-striking normal faults became either inactive (XJ33) or sharply decreased their activity (e.g., EP17, PY4, XJ23, and LF15). Besides, the inactive ENE-striking XJ33 fault, which reactivated the PFS2 in the Syn-rift stage 1, was crosscut by the new EW-striking XJ33S fault in the Syn-rift stage 2, which reactivated a pre-existing fault of the PFS1 that

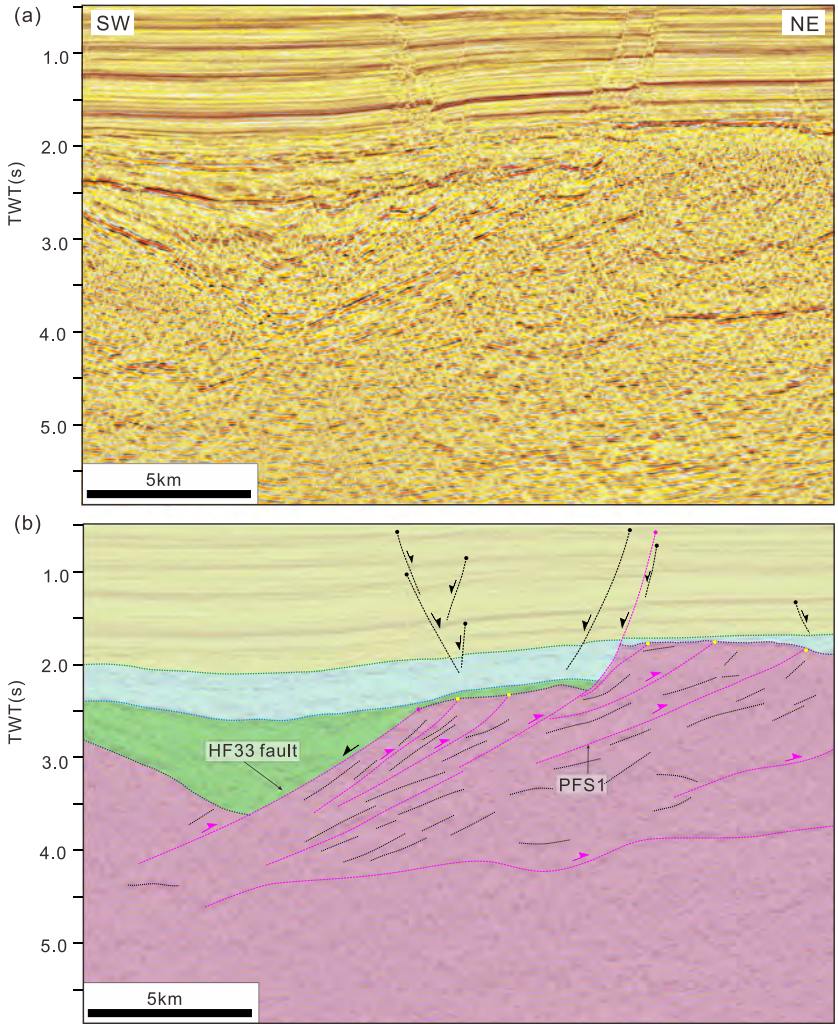

Figure 8. (a-b) Uninterpreted and interpreted seismic sections (see Figure 2b for location) across the eastern WNW-striking portion of the HF33 fault. This section is SW-NE orientated. This portion of the HF33 fault reactivated a pre-existing fault of the PFS1.

was rooted in the foot-wall basement of the XJ33F fault (Figure 5). These combined changes in fault activity and depocenter development during the second rifting phase reflected the preferential reactivation of the PFS1 during the second rifting phase.

5. Discussion

5.1. Changes in the Extension Direction During the Two Rifting Phases in the SCS Area

For rift basin studies, the identification of the extension direction associated with each rifting phase is significant, since it may enable the correlation of the rifting kinematics to the surrounding regional changes in relative plate motions. However, the extension direction during rifting is not easily determined, since pre-existing structures like faults, ductile planes, shear zones, foliations, and anisotropies in the pre-rift basement are expected to influence the rift development. Therefore, it is not convincing to determine the extension direction just based on the strike of rifting faults.

The extension direction during the two above-mentioned rifting phases in the SCS area is not well determined, and two main documented scenarios existed. Several authors suggested a clockwise rotation of the extension direction from NNW-SSE (or described as NW-SE) in the first rifting phase to N-S in the second rifting phase on the basis of orientation analyses of the Cenozoic rifting structures (e.g., Zhou et al., 1995; Hu et al., 2016; Zhang et al., 2018; Deng et al., 2018). On the contrary, few authors considered a constant

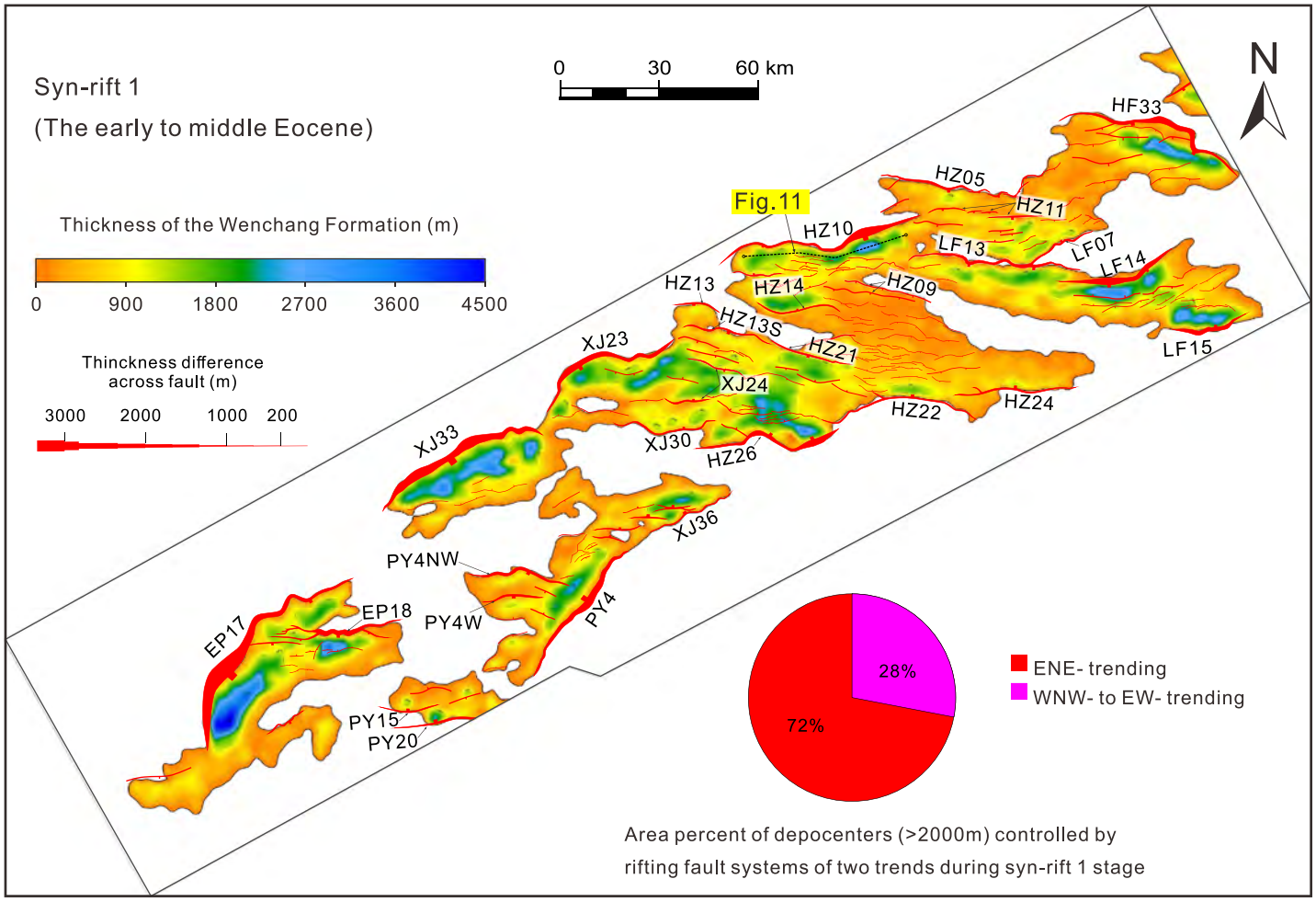

Figure 9. The isopach map of the Syn-rift 1 Wenchang Formation. Main active faults during this rifting phase are superimposed on the map allowing the assessment of both the depocenter development and fault activity. The width of fault polygon is in proportion to the thickness difference across fault. Area percent are illustrated for depocenters with more than 2000m thickness deposition, controlled by the ENE-striking and WNW- to EW-striking normal fault systems, respectively.

N-S extension direction from the Syn-rift 1 to the Syn-rift 2 stage throughout the early to the middle Cenozoic (e.g., Chan et al., 2010; Savva et al., 2014). This controversial issue in the SCS area to some extent may have influenced our understanding of the dynamic origin and kinematic development of the SCS opening.

It has been well studied that the degree to which pre-existing faults in a certain area can undergo reactivation largely depends on their orientations relative to the extension direction, though as was mentioned above the size, dip angle, and spacing of the pre-existing faults may also exert a significant influence on the degree of reactivation (e.g., Bonini et al., 2015, 2016; Corti et al., 2006, 2007; Morley, 2010; Morley et al., 2004; Phillips et al., 2016; Reilly et al., 2016). Numerical and analog models suggested that under a given extension direction, large depocenters are predicted to form in pre-existing weak zones mostly orthogonal to the extension direction, while smaller depocenters will form along the oblique weak zones (e.g., Corti et al., 2007). Conversely, for an area where pre-existing fault orientations are known, the rough extension direction can be derived based on to what degree and how the pre-existing fault systems have been reactivated during the rifting process. Therefore, by analyzing the reactivation patterns of the two pre-existing fault systems in the study area (Figure 12a), we may get convincing evidence for determining the extension direction during the two rifting phases in the SCS area, in the context of the two previously proposed scenarios mentioned above. The preferential reactivation of the PFS2 and dominant activity of the ENE-striking rifting faults during the first rifting phase suggest that the ENE-striking PFS2 was optimally oriented with respect to the

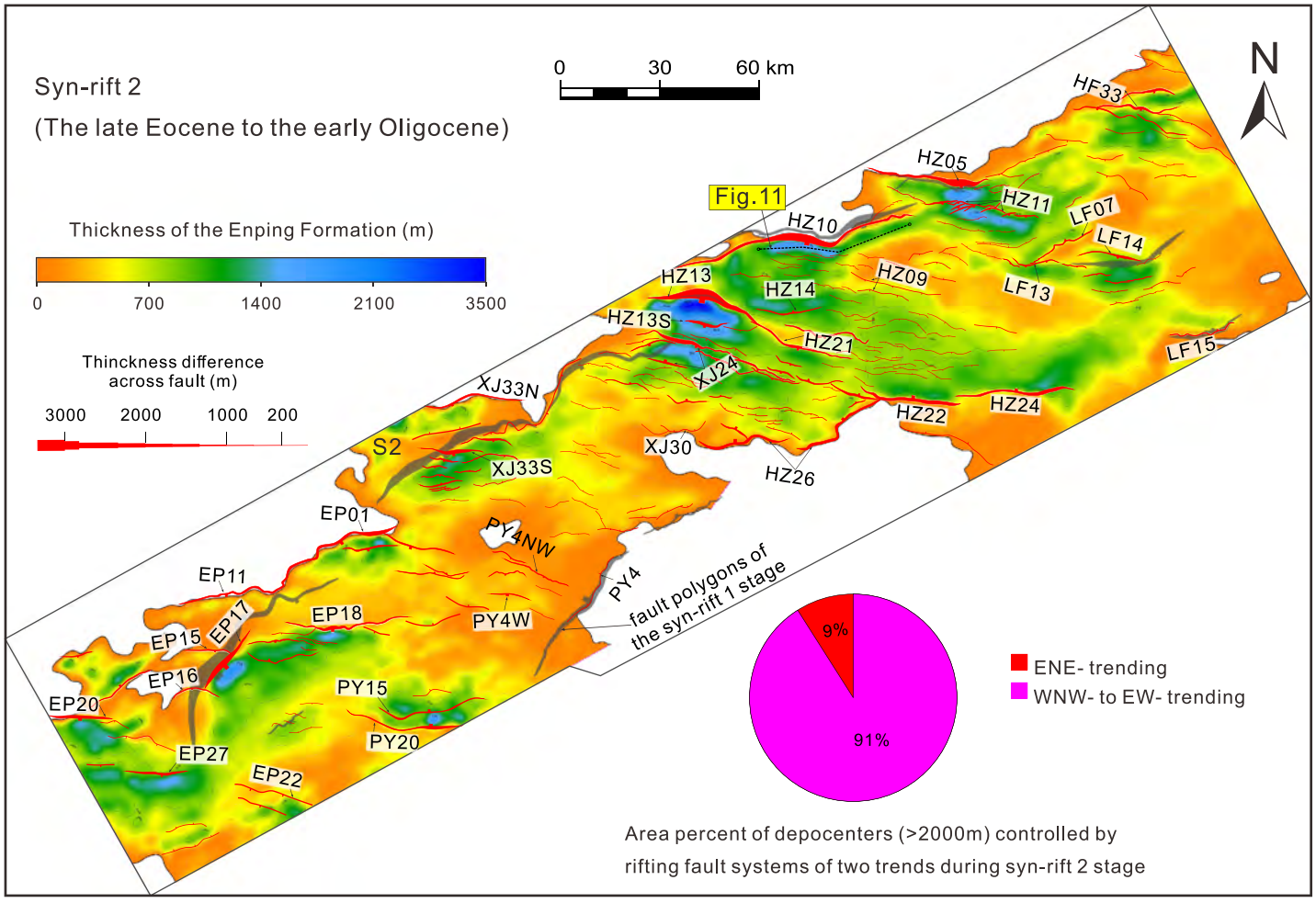

Figure 10. The isopach map of the Syn-rift 2 Enping Formation. Main active faults during this rifting phase are superimposed on the map. Fault polygons of some major bounding faults of the Syn-rift 1 stage (in translucent grey) are also superimposed for the sake of comparison; these fault either become died or largely increase their activity during the Syn-rift 2 stage. Area percent are illustrated for depocenters with more than 2,000 m thickness deposition, controlled by ENE-striking and WNW- to EW-striking normal faults, respectively. Notice the change of main active faults and migration of depocenters with respect to those of the Syn-rift 1 stage in Figure 10.

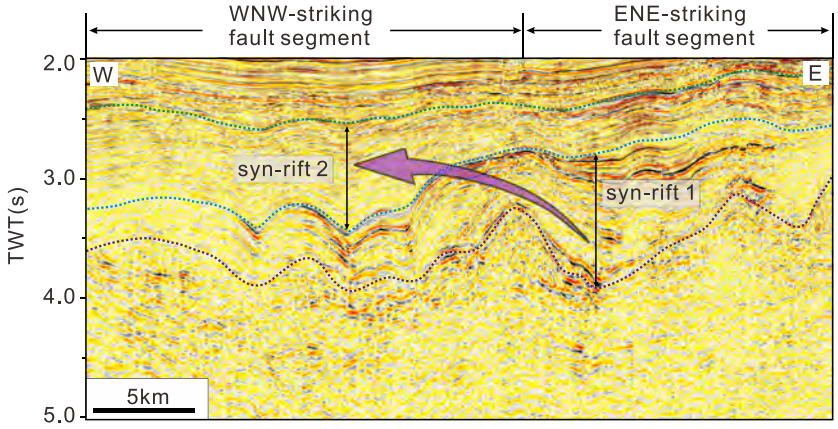

Figure 11. An arbitrary seismic line along the hanging wall of the HZ10 fault (see location in Figures 9 and 10), showing the depocenter migration at the base of the HZ10 fault from its eastern ENE-striking segment in the Syn-rift 1 stage to western WNW-striking fault segment in the Syn-rift 2 stage.

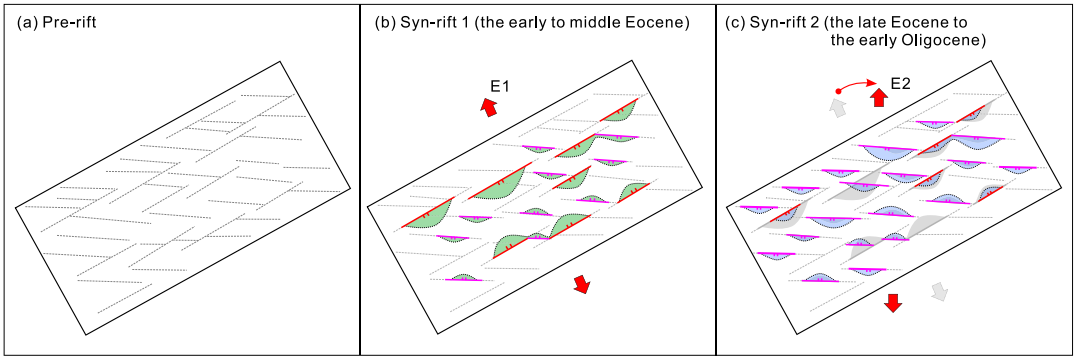

Figure 12. Simplified model (not to scale) showing influence of pre-existing basement faults on rift evolution in the proximal domain of the northern SCS margin. (a) Two pre-existing basement fault systems: the WNW- to EW-striking fault system (PFS1) and the ENE-striking fault system (PFS2). (b) The extension direction in the first rifting phase during the early to middle Eocene was NNW-SSE. Both the two pre-existing fault systems were reactivated, resulting in development of rifting faults of two orientations (red and pink fault groups) and their associated depocenters (filling in light green). The PFS2 was more prone to be reactivated during this rifting phase, and the large and thick depocenters were mainly controlled by the ENE-striking bounding faults. (c) During the second rifting phase in the late Eocene to the early Oligocene, the extension direction rotated to N-S. More pre-existing faults of the PFS1 were reactivated, and the WNW- to EW-striking rifting faults became more active and controlled the development of the main depocenters (filling in light blue). On the contrary, many of the Syn-rift 1 ENE-striking bounding faults became died or less active (in grey) and could even be crosscut by the WNW- to EW-striking rifting faults.

regional extension direction, which seems to support a NNW-SSW extension direction rather than a N-S direction of extension during this stage (Figure 12b). However, during the second rifting phase, the decrease of activity of the earlier ENE-striking rifting faults and increase of activity of the WNW- to EW-striking rifting faults, which reactivated the PFS1, suggest a change of the extension direction, which may have rotated to N-S and become more orthogonal to the PFS1 (Figure 12c). Therefore, this study supports the idea of a clockwise rotation of the extension direction from NNW-SSE in the early to middle Eocene rifting phase to N-S in the late Eocene to the early Oligocene rifting phase in the SCS area. Interestingly, some studies on the post-rift faults in the northern SCS margin have revealed a NNE-SSW extensional regime during the syn-spreading stage following the syn-rift stage (Deng et al., 2018; Ye et al., 2017). Such continuous clockwise rotation of the extension direction from the two-phase syn-rift extension to the syn-spreading extension seems to imply the contribution of the collision of the Indian plate with the Eurasian plate and the extrusion of the Indochina block to the opening of the SCS, which is one of the most popular dynamic models for the SCS development (e.g., Briais et al., 1993; Leloup et al., 2001; Pigott & Ru, 1994; Replumaz & Tapponnier, 2003; Tapponnier et al., 1986, 1990).

The map pattern of the rift-related faults as derived from this study are also feasible to some alternative interpretations that should be discussed. In particular, it has been shown in previous studies that similar map patterns can arise from a single, rather than multiple, extensional events (Reeve et al., 2015). For example, two extensional fault trends can often develop under the influence of a single extensional event/direction in oblique rift systems due to the existence of pre-existing weaknesses zones oblique to the extension direction (Corti, 2008; McClay et al., 2002; McClay & White, 1995; Tron & Brun, 1991). Similarly, in rift systems where one extensional fault system is associated with the reactivation of inherited basement faults of certain directions or with the local re-orientation of extension vectors, a second fault system can develop perpendicular to the extension direction (Henza et al., 2011; Samsu et al., 2019). However, we stress that the well-proven existence of two pre-existing basement fault systems with different orientations (Ye, Mei, Shi, Camanni, et al., 2018) and the overlying development of two distinct rifting fault systems with similar orientations, as well as the clear evidence of reactivation of the two pre-existing fault systems from seismic sections, strongly support the idea that both the recognized rift-related fault systems mainly developed as the result of fault reactivation under the influence of two distinct extension directions.

5.2. Implications for Understanding the Rift Development Across the SCS Area

Pre-existing basement structures, mainly inherited from the late Mesozoic surrounding plate tectonics (Ye, Mei, Shi, Camanni, et al., 2018), should not be unique to the proximal domain and are likely to be regionally

extendable across the whole SCS area. The proximal domain of the SCS margin (i.e., the study area in this paper) is located in the landward, outboard area of the rifted margin, where extensional strain is low. Relatively shallow burial depth of the basement in this area along with the low Cenozoic extension make it feasible to identify pre-existing structures and analyze their influence using basin-scale seismic reflection data. However, for the inboard region of the rifted margin, such as in the hyperextended and distal domains (Figure 1a), a similar work is more difficult because of the intense influence of Cenozoic extension and the limited resolution of geophysical data in deep part of the basin. As a result, some previous studies on the rift evolution in these inboard regions have put more emphasis on the Cenozoic tectonic processes including the Cenozoic faulting, crust thinning, and magmatism, without taking into account the influence of pre-existing structures. However, Cenozoic tectonic processes alone usually could not well explain diverse rift structure along the rift axis and the origin of many peculiar structural geometries. For example, distinct structural trends (NE-ENE-, EW-WNW-, and NNW-trending) also exist in the southern distal basin (the Zhu II Depression) though the influence of pre-existing basement structures have not been confirmed yet (Yang et al., 2018; Zhou et al., 2018). In fact, basement structures in the present inboard northern SCS margin could be even more complex than that in the outboard area as described in this study since it was more closed to the southern plate margin during the Mesozoic. The influence of pre-existing structures on rift development in the proximal domain of the northern SCS margin documented in this study implies that preexisting structures may also have played a key role during rifting evolution in other zones across the SCS margin and deserve more attention in future studies. Remarkably, after the IODP expeditions 368/369 in 2017, the SCS margin was confirmed to be a special rifted margin that differs from both traditional magma-poor and magma-rich margins for the inexistence of the expected exhumed mantle in its distal part and the rapid transition from rifting to igneous crustal accretion, and the origin of this specific margin was speculated to be likely influenced by pre-existing nature of the lithosphere (Larsen et al., 2018). An enhanced study on how pre-existing structures influence rifting evolution will advance not only understanding of the rift basin structure, which will be beneficial to petroleum exploration, but also a better understanding of the development mechanism for the special rifted margin of the SCS.

6. Conclusions

1. The overall rift architecture in the proximal domain of the northern South China Sea margin is mainly controlled by the selective reactivation of two pre-existing fault systems within basement, the WNW- to EW-striking PFS1 and the ENE-striking PFS2. The extensional reactivation of both the two pre-existing fault systems led to the coeval development of ENE- and WNW- to EW-striking rifting faults, and also some complex "Z" or "V"-shape faults.
2. From the Rifting stage 1 to Rifting stage 2, the degrees of activity of the two rifting fault systems changed, and the main depocenters migrated from mainly being controlled by the ENE-striking normal faults to being controlled by the WNW- to EW-striking normal faults.
3. The different degrees of activity of the two rifting fault systems during the two rifting phases was influenced by different degrees of reactivation of the two pre-existing fault systems, which supports the idea of a clockwise rotation of the extension direction from NNW-SSE in the early to middle Eocene rifting phase to N-S in the late Eocene to the early Oligocene rifting phase.
4. The influence of pre-existing structures on rift development in the proximal domain of the northern SCS margin documented in this study implies that pre-existing structures may also have played a key role during rifting evolution in other areas across the SCS margin and deserve more attention in future studies.

Acknowledgments
This study was financially supported by the Major National Science and Technology Programs, China (No. 2016ZX05026-003-001). Qing Ye acknowledges the China Scholarship Council for supporting his 1-year study in University College Dublin from November 2017 to November 2018 and really appreciate Conrad Childs for his help and guidance during this period. The Shenzhen Branch of the China National Offshore Oil Corporation is thanked for providing seismic reflection data presented in this study. The authors acknowledge the thoughtful and useful reviews provided by Andrew Cullen, Jonny Wu, Jiawang Ge, and an anonymous reviewer that helped to improve the early versions of this manuscript. We thank the Editor John Geissman and Associate Editor Luc Lavier for handling the manuscript. All the data used in this study are listed in the figures or archived in Figshare repository (https://doi.org/10.6084/m9.figshare.11661477.v1).

References

Autin, J., Bellahsen, N., Leroy, S., Husson, L., Beslier, M. O., & d'Acremont, E. (2013). The role of structural inheritance in oblique rifting: Insights from analogue models and application to the Gulf of Aden. *Tectonophysics*, *607*, 51–64. https://doi.org/10.1016/j.tecto.2013.05.041

Bao, X., Ji, Y., Hu, Y., & Zong, Y. (2017). Geochemical characteristics, origins, and model of lacustrine source rocks in the Zhu 1 depression, eastern Pearl River Mouth Basin, South China Sea. *AAPG Bulletin*, *101*(9), 1543–1564. https://doi.org/10.1306/11071614117

Bird, P. C., Cartwright, J. A., & Davies, T. L. (2015). Basement reactivation in the development of rift basins: an example of reactivated Caledonide structures in the West Orkney Basin. *Journal of the Geological Society*, *172*(1), 77–85. https://doi.org/10.1144/jgs2013-098

Bladon, A. J., Clarke, S. M., & Burley, S. D. (2015). Complex rift geometries resulting from inheritance of pre-existing structures: Insights and regional implications from the Barmer Basin rift. *Journal of Structural Geology*, *71*, 136–154. https://doi.org/10.1016/j.jsg.2014.09.017

Bonini, L., Basili, R., Toscani, G., Burrato, P., Seno, S., & Valensise, G. (2015). The role of pre-existing discontinuities in the development of extensional faults: an analog modeling perspective. *Journal of structural geology*, *74*, 145–158. https://doi.org/10.1016/j.jsg.2015.03.004

Bonini, L., Basili, R., Toscani, G., Burrato, P., Seno, S., & Valensise, G. (2016). The effects of pre-existing discontinuities on the surface expression of normal faults: Insights from wet-clay analog modeling. *Tectonophysics*, *684*, 157–175. https://doi.org/10.1016/j.tecto.2015.12.015

Briais, A., Patriat, P., & Tapponnier, P. (1993). Updated interpretation of magnetic anomalies and seafloor spreading stages in the South China Sea: Implications for the Tertiary tectonics of Southeast Asia. *Journal of Geophysical Research: Solid Earth*, *98*(B4), 6299–6328. https://doi.org/10.1029/92JB02280

Chan, L. S., Shen, W., & Pubellier, M. (2010). Polyphase rifting of greater Pearl River Delta region (South China): Evidence for possible rapid changes in regional stress configuration. *Journal of Structural Geology*, *32*(6), 746–754. https://doi.org/10.1016/j.jsg.2010.04.015

Corti, G. (2008). Control of rift obliquity on the evolution and segmentation of the main Ethiopian rift. *Nature Geoscience*, *1*(4), 258.

Corti, G., Lucia, S., Bonini, M., Sani, F., & Mazzarini, F. (2006). Interaction between normal faults and pre-existing thrust systems in analogue models. *Geological Society, London, Special Publications*, *253*(1), 65–78. https://doi.org/10.1144/GSL.SP.2006.253.01.03

Corti, G., van Wijk, J., Cloetingh, S., & Morley, C. K. (2007). Tectonic inheritance and continental rift architecture: Numerical and analogue models of the East African Rift system. *Tectonics*, *26*(6). https://doi.org/10.1029/2006TC002086

Daly, M. C., Chorowicz, J., & Fairhead, J. D. (1989). Rift basin evolution in Africa: The influence of reactivated steep basement shear zones. *Geological Society, London, Special Publications*, *44*(1), 309–334. https://doi.org/10.1144/GSL.SP.1989.044.01.17

Deng, P. (2018). *The Nature and Tectonic Transition of the multiphase rifting in the Northern Margin of the South China Sea: Based on the Study of the Zhu I Depression in Pearl River Mouth Basin (in Chinese with English abstract)*. Wuhan: Ph.D. thesis, China University of Geosciences.

Deng, P., Mei, L., Liu, J., Zheng, J., Liu, M., Cheng, Z., & Guo, F. (2018). Episodic normal faulting and magmatism during the syn-spreading stage of the Baiyun sag in Pearl River Mouth Basin: Response to the multi-phase seafloor spreading of the South China Sea. *Marine Geophysical Research*, *40*(1), 33–50. https://doi.org/10.1007/s11001-018-9352-9

Expedition 349 Scientists (2014). *South China Sea tectonics: Opening of the South China Sea and its implications for southeast Asian tectonics, climates, and deep mantle processes since the late Mesozoic* (p. 349). International Ocean Discovery Program Preliminary Report. https://doi.org/10.14379/iodp.pr.349.2014

Faccenna, C., Nalpas, T., Brun, J. P., Davy, P., & Bosi, V. (1995). The influence of pre-existing thrust faults on normal fault geometry in nature and in experiments. *Journal of Structural Geology*, *17*(8), 1139–1149. https://doi.org/10.1016/0191-8141(95)00008-2

Fazlikhani, H., Fossen, H., Gawthorpe, R. L., Faleide, J. I., & Bell, R. E. (2017). Basement structure and its influence on the structural configuration of the northern North Sea rift. *Tectonics*, *36*(6), 1151–1177. https://doi.org/10.1002/2017TC004514

Franke, D., Savva, D., Pubellier, M., Steuer, S., Mouly, B., Auxietre, J. L., et al. (2014). The final rifting evolution in the South China Sea. *Marine and Petroleum Geology*, *58*, 704–720. https://doi.org/10.1016/j.marpetgeo.2013.11.020

Gawthorpe, R. L., & Leeder, M. R. (2000). Tectono-sedimentary evolution of active extensional basins. *Basin Research*, *12*(3-4), 195–218, et al. https://doi.org/10.1111/j.1365-2117.2000.00121.x

Ge, J., Zhu, X., Yu, F., Jones, B. G., & Tao, W. (2018). Controls of faulting on synrift infill patterns in the Eocene PY4 Sag, Pearl River Mouth Basin. *South China Sea. Australian Journal of Earth Sciences*, *66*(1), 111–132. https://doi.org/10.1080/08120099.2018.1512524

Ge, J. W., Zhu, X. M., Zhang, X. T., Jones, B. G., Yu, F. S., Niu, Z. C., & Li, M. (2017). Tectono-stratigraphic evolution and hydrocarbon exploration in the Eocene Southern Lufeng Depression, Pearl River Mouth Basin, South China Sea. *Australian Journal of Earth Sciences*, *64*(7), 931–956. https://doi.org/10.1080/08120099.2017.1370613

Gibson, G. M., Totterdell, J. M., White, L. T., Mitchell, C. H., Stacey, A. R., Morse, M. P., & Whitaker, A. (2013). Pre-existing basement structure and its influence on continental rifting and fracture zone development along Australia's southern rifted margin. *Journal of the Geological Society*, *170*(2), 365–377. https://doi.org/10.1144/jgs2012-040

Hayes, D. E., & Nissen, S. S. (2005). The South China sea margins: Implications for rifting contrasts. *Earth and Planetary Science Letters*, *237*(3-4), 601–616. https://doi.org/10.1016/j.epsl.2005.06.017

Henza, A. A., Withjack, M. O., & Schlische, R. W. (2011). How do the properties of a pre-existing normal-fault population influence fault development during a subsequent phase of extension? *Journal of Structural Geology*, *33*(9), 1312–1132. https://doi.org/10.1016/j.jsg.2011.06.010

Hesheng, S., Dai Yiding, L. L., Hang, J., Jing, B., & Hongbo, L. (2015). Geological characteristics and distribution model of oil and gas reservoirs in Zhu-I depression. Pearl River Mouth Basin. *Acta Petrolei Sinica*, *36*(2), 120–133 (in Chinese with English abstract). https://doi.org/10.7623/syxb2015S2011

Hu, Y., Wu, Z. P., Zhong, Z. H., Zhang, J. T., Yu, W. G., Wang, G. Z., et al. (2016). Characterization and genesis of the Middle and Late Eocene tectonic changes in Zhu 1 Depression of Pearl River Mouth Basin. *Oil & Gas Geology*, *37*(5), 779–785 (in Chinese with English abstract). https://doi.org/10.11743/ogg20160518

Jian, Z., Larsen, H. C., Alvarez Zarikian, C. A., & the Expedition 368 Scientists (2018). *Expedition 368 Preliminary Report: South China Sea Rifted Margin*. International Ocean Discovery Program. https://doi.org/10.14379/iodp.pr.368.2018

Katumwehe, A. B., Abdelsalam, M. G., & Atekwana, E. A. (2015). The role of pre-existing Precambrian structures in rift evolution: The Albertine and Rhino grabens, Uganda. *Tectonophysics*, *646*, 117–129. https://doi.org/10.1016/j.tecto.2015.01.022

Kharazizadeh, N., Schellart, W. P., Duarte, J. C., & Hall, M. (2017). Influence of lithosphere and basement properties on the stretching factor and development of extensional faults across the Otway Basin, southeast Australia. *Marine and Petroleum Geology*, *88*, 1059–1077. https://doi.org/10.1016/j.marpetgeo.2017.08.034

Larsen, H. C., Mohn, G., Nirrengarten, M., Sun, Z., Stock, J., Jian, Z., et al. (2018). Rapid transition from continental breakup to igneous oceanic crust in the South China Sea. *Nature Geoscience*, *11*(10), 782–789. https://doi.org/10.1038/s41561-018-0198-1

Leloup, P. H., Arnaud, N., Lacassin, R., Kienast, J. R., Harrison, T. M., Trong, T. T., et al. (2001). New constraints on the structure, thermochronology, and timing of the Ailao Shan-Red River shear zone, SE Asia. *Journal of Geophysical Research: Solid Earth*, *106*(B4), 6683–6732. https://doi.org/10.1029/2000JB900322

Li, C. F., Xu, X., Lin, J., Sun, Z., Zhu, J., Yao, Y., et al. (2014). Ages and magnetic structures of the South China Sea constrained by deep tow magnetic surveys and IODP Expedition 349. *Geochem. Geophys. Geosyst.*, *15*(12), 4958–4983. https://doi.org/10.1002/2014GC005567

Li, F., Sun, Z., & Yang, H. (2018). Possible spatial distribution of the Mesozoic volcanic arc in the present-day South China Sea continental margin and its tectonic implications. *Journal of Geophysical Research: Solid Earth*, *123*(8), 6215–6235. https://doi.org/10.1029/2017JB014861

Li, P. L. (1993). Cenozoic tectonic movement in the Pearl River Mouth Basin China. *Offshore Oil Gas (Geology)*, *7*(6), 11–17. (in Chinese with English abstract)

Li, S., Lin, C., Zhang, Q., Yang, S., & Wu, P. (1999). Episodic rifting of continental marginal basins and tectonic events since 10 Ma in the South China Sea. *Chinese Science Bulletin*, *44*(1), 10–23.

Liu, Q. H., Zhu, H. T., Shu, Y., Zhu, X. M., Yang, X. H., Chen, L., et al. (2016a). Provenance identification and sedimentary analysis of the beach and bar systems in the Palaeogene of the Enping Sag, Pearl River Mouth Basin, South China Sea. *Marine and Petroleum Geology*, *70*, 251–272. https://doi.org/10.1016/j.marpetgeo.2015.12.002

Liu, Q. H., Zhu, H. T., Shu, Y., Zhu, X. M., Yang, X. H., Tan, M., et al. (2016b). Effects of low-to high-angle normal faults on sedimentary architectures in the Eocene Wenchang Formation, Enping Sag, Pearl River Mouth Basin, South China Sea. *Australian Journal of Earth Sciences*, *63*(7), 903–922. https://doi.org/10.1080/08120099.2016.1257512

Lüdmann, T., Wong, H. K., & Wang, P. (2001). Plio–Quaternary sedimentation processes and neotectonics of the northern continental margin of the South China Sea. *Marine Geology*, *172*(3-4), 331–358. https://doi.org/10.1016/S0025-3227(00)00129-8

Manatschal, G., Lavier, L., & Chenin, P. (2015). The role of inheritance in structuring hyperextended rift systems: Some considerations based on observations and numerical modeling. *Gondwana Research*, *27*(1), 140–164. https://doi.org/10.1016/j.gr.2014.08.006

McClay, K. R., Dooley, T., Whitehouse, P., & Mills, M. (2002). 4-D evolution of rift systems: Insights from scaled physical models. *AAPG bulletin*, *86*(6), 935–959.

McClay, K. R., & White, M. J. (1995). Analogue modelling of orthogonal and oblique rifting. *Marine and Petroleum Geology*, *12*(2), 137–151. https://doi.org/10.1016/0264-8172(95)92835-K

Morley, C. K. (2010). Stress re-orientation along zones of weak fabrics in rifts: An explanation for pure extension in 'oblique' rift segments? *Earth and Planetary Science Letters*, *297*(3-4), 667–673. https://doi.org/10.1016/j.epsl.2010.07.022

Morley, C. K. (2016a). Major unconformities/termination of extension events and associated surfaces in the South China Seas: Review and implications for tectonic development. *Journal of Asian Earth Sciences*, *120*, 62–86. https://doi.org/10.1016/j.jseaes.2016.01.013

Morley, C. K. (2016b). The impact of multiple extension events, stress rotation and inherited fabrics on normal fault geometries and evolution in the Cenozoic rift basins of Thailand. *Geological Society, London, Special Publications*, *439*(1), 413–445. https://doi.org/10.1144/SP439.3

Morley, C. K., Haranya, C., Phoosongsee, W., Pongwapee, S., Kornsawan, A., & Wonganan, N. (2004). Activation of rift oblique and rift parallel pre-existing fabrics during extension and their effect on deformation style: Examples from the rifts of Thailand. *Journal of Structural Geology*, *26*(10), 1803–1829. https://doi.org/10.1016/j.jsg.2004.02.014

Peron-Pinvidic, G., Manatschal, G., & Osmundsen, P. T. (2013). Structural comparison of archetypal Atlantic rifted margins: A review of observations and concepts. *Marine and Petroleum Geology*, *43*, 21–47. https://doi.org/10.1016/j.marpetgeo.2013.02.002

Phillips, T. B., Jackson, C. A., Bell, R. E., Duffy, O. B., & Fossen, H. (2016). Reactivation of intrabasement structures during rifting: A case study from offshore southern Norway. *Journal of Structural Geology*, *91*, 54–73. https://doi.org/10.1016/j.jsg.2016.08.008

Pigott, J. D., & Ru, K. (1994). Basin superposition on the northern margin of the South China Sea. *Tectonophysics*, *235*(1-2), 27–50. https://doi.org/10.1016/0040-1951(94)90015-9

Reeve, M. T., Bell, R. E., Duffy, O. B., Jackson, C. A. L., & Sansom, E. (2015). The growth of non-colinear normal fault systems; What can we learn from 3D seismic reflection data? *Journal of Structural Geology*, *70*, 141–155. https://doi.org/10.1016/j.jsg.2014.11.007

Reilly, C., Nicol, A., & Walsh, J. (2016). Importance of pre-existing fault size for the evolution of an inverted fault system. *Geological Society, London, Special Publications*, *439*(1), 447–463. https://doi.org/10.1144/SP439.2

Replumaz, A., & Tapponnier, P. (2003). Reconstruction of the deformed collision zone between India and Asia by backward motion of lithospheric blocks. *Journal of Geophysical Research: Solid Earth*, *108*(B6). https://doi.org/10.1029/2001JB000661

Rotevatn, A., Kristensen, T. B., Ksienzyk, A. K., Wemmer, K., Henstra, G. A., Midtkandal, I., et al. (2018). Structural inheritance and rapid rift-length establishment in a multiphase rift: The East Greenland rift system and its Caledonian orogenic ancestry. *Tectonics*, *37*(6), 1858–1875. https://doi.org/10.1029/2018TC005018

Ru, K., & Pigott, J. D. (1986). Episodic rifting and subsidence in the South China Sea. *AAPG Bulletin*, *70*(9), 1136–1155. https://doi.org/10.1306/94886A8D-1704-11D7-8645000102C1865D

Samsu, A., Cruden, A. R., Hall, M., Micklethwaite, S., & Denyszyn, S. W. (2019). The influence of basement faults on local extension directions: Insights from potential field geophysics and field observations. *Basin Research*, *31*(4), 782–807. https://doi.org/10.1111/bre.12344

Savva, D., Pubellier, M., Franke, D., Chamot-Rooke, N., Meresse, F., Steuer, S., & Auxietre, J. L. (2014). Different expressions of rifting on the South China Sea margins. *Marine and Petroleum Geology*, *58*, 579–598. https://doi.org/10.1016/j.marpetgeo.2014.05.023

Sibson, R. H. (1985). A note on fault reactivation. *Journal of Structural Geology*, *7*(6), 751–754. https://doi.org/10.1016/0191-8141(85)90150-6

Sun, Z., Stock, J., Klaus, A., & the Expedition 367 Scientists (2018). *Expedition 367 Preliminary Report: South China Sea Rifted Margin*. International Ocean Discovery Program. https://doi.org/10.14379/iodp.pr.367.2018

Sun, Z., Xu, Z., Sun, L., Pang, X., Yan, C., Li, Y., et al. (2014). The mechanism of post-rift fault activities in Baiyun sag, Pearl River Mouth basin. *Journal of Asian Earth Sciences*, *89*, 76–87. https://doi.org/10.1016/j.jseaes.2014.02.018

Tapponnier, P., Lacassin, R., Leloup, P. H., Schärer, U., Dalai, Z., Haiwei, W., et al. (1990). The Ailao Shan/Red River metamorphic belt: Tertiary left-lateral shear between Indochina and South China. *Nature*, *343*(6257), 431.

Tapponnier, P., Peltzer, G., & Armijo, R. (1986). On the mechanics of the collision between India and Asia. *Geological Society, London, Special Publications*, *19*(1), 113–157. https://doi.org/10.1144/GSL.SP.1986.019.01.07

Tron, V., & Brun, J. P. (1991). Experiments on oblique rifting in brittle-ductile systems. *Tectonophysics*, *188*(1-2), 71–84. https://doi.org/10.1016/0040-1951(91)90315-J

Tsai, C. H., Hsu, S. K., Yeh, Y. C., Lee, C. S., & Xia, K. (2004). Crustal thinning of the northern continental margin of the South China Sea. *Marine Geophysical Researches*, *25*(1-2), 63–78. https://doi.org/10.1007/s11001-005-0733-5

Wang, W., Ye, J. R., Yang, X. H., Shi, H. S., Shu, Y., & Wu, J. (2015). Sediment provenance and depositional response to multistage rifting, Paleogene, Huizhou Depression, Pearl River Mouth Basin. *Earth Sci.*, *40*(6), 1061–1071. (in Chinese with English abstract) https://doi.org/10.3799/dqkx.2015.088

Williams, G. D., Powell, C. M., & Cooper, M. A. (1989). Geometry and kinematics of inversion tectonics. *Geological Society, London, Special Publications*, *44*(1), 3–15. https://doi.org/10.1144/GSL.SP.1989.044.01.02

Wu, S., Gao, J., Zhao, S., Lüdmann, T., Chen, D., & Spence, G. (2014). Post-rift uplift and focused fluid flow in the passive margin of northern South China Sea. *Tectonophysics*, *615*, 27–39. https://doi.org/10.1016/j.tecto.2013.12.013

Wu, Z., Zhu, W., Shao, L., & Xu, C. (2016). Sedimentary facies and the rifting process during the late Cretaceous to early Oligocene in the northern continental margin, South China Sea. *Interpretation*, *4*(3), SP33–SP45. https://doi.org/10.1190/int-2015-0163.1

Yan, P., Zhou, D., & Liu, Z. S. (2001). A crustal structure profile across the northern continental margin of the South China Sea. *Tectonophysics*, *338*(1), 1–21. https://doi.org/10.1016/S0040-1951(01)00062-2

Yang, L., Ren, J., McIntosh, K., Pang, X., Chao, L., & Zhao, Y. (2018). The structure and evolution of deepwater basins in the distal margin of the northern South China Sea and their implications for the formation of the continental margin. *Marine and Petroleum Geology*, *92*, 234–254. https://doi.org/10.1016/j.marpetgeo.2018.02.032

Ye, Q., Mei, L., Shi, H., Camanni, G., Shu, Y., Wu, J., et al. (2018). The Late Cretaceous tectonic evolution of the South China Sea area: An overview, and new perspectives from 3D seismic reflection data. *Earth-science reviews*, *187*, 186–204. https://doi.org/10.1016/j.earscirev.2018.09.013

Ye, Q., Mei, L., Shi, H., Shu, Y., Camanni, G., & Wu, J. (2018). A low-angle normal fault and basement structures within the Enping Sag, Pearl River Mouth Basin: Insights into late Mesozoic to early Cenozoic tectonic evolution of the South China Sea area. *Tectonophysics*, *731*, 1–16. https://doi.org/10.1016/j.tecto.2018.03.003

Ye, Q., Shi, H. S., Mei, L. F., Shu, Y., Liu, H. L., Tian, W., & Yan, H. (2017). Post-rift Faulting Migration, transition and Dynamics in Zhu I Depression, Pearl River Mouth Basin. *Earth Sci.*, *42*(1), 105–118 (in Chinese with English abstract). https://doi.org/10.3799/dqkx.2017.008

Yi, H., Zhang, L., & Lin, Z. (2012). Mesozoic tectonic framework and basin distribution characteristics of northern margin of South China Sea. *Pet. Geol. Exp.*, *34*(4), 388–394. (in Chinese with English abstract)

Zhang, Y., Sun, Z., Zhou, D., Guo, X., Shi, X., Wu, X., & Pang, X. (2008). Stretching characteristics and its dynamic significance of the northern continental margin of South China Sea. *Science in China Series D: Earth Sciences*, *51*(3), 422–430. https://doi.org/10.1007/s11430-008-0019-2

Zhang, Z. Y., Qi, J. F., & Wu, J. F. (2018). Cenozoic faults systems and its geodynamics of the continental margin basins in the northern of South China Sea. *Earth Science*, *44*(2), 603–625. (in Chinese with English abstract). https://doi.org/10.3799/dqkx.2018.542

Zhou, D., Ru, K., & Chen, H. Z. (1995). Kinematics of Cenozoic extension on the South China Sea continental margin and its implications for the tectonic evolution of the region. *Tectonophysics*, *251*(1-4), 161–177. https://doi.org/10.1016/0040-1951(95)00018-6

Zhou, Z., Mei, L., Liu, J., Zheng, J., Chen, L., & Hao, S. (2018). Continentward-dipping detachment fault system and asymmetric rift structure of the Baiyun Sag, northern South China Sea. *Tectonophysics*, *726*, 121–136. https://doi.org/10.1016/j.tecto.2018.02.002

Zhu, H., Li, S., Shu, Y., Yang, X., & Mei, L. (2016). Applying seismic geomorphology to delineate switched sequence stratigraphic architecture in lacustrine rift basins: An example from the Pearl River Mouth Basin, northern South China Sea. *Marine and Petroleum Geology*, *78*, 785–796. https://doi.org/10.1016/j.marpetgeo.2015.12.013